Effect of nozzle sizes on jet impingement heat transfer in He-cooled divertor

Boštjan Končar, Prachai Norajitra, Klemen Oblak

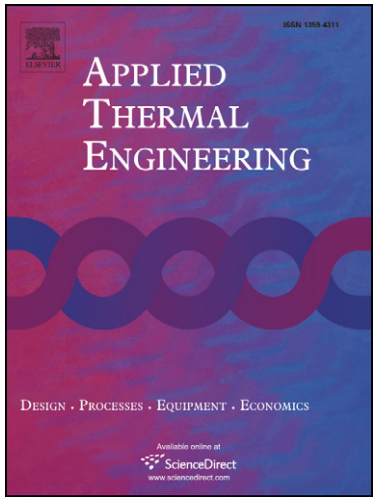

Effect of nozzle sizes on jet impingement heat transfer in He-cooled divertor

Boštjan Končar, Prachai Norajitra, Klemen Oblak

PII: S1359-4311(09)00346-9
DOI: 10.1016/j.applthermaleng.2009.11.018
Reference: ATE 2936

To appear in: *Applied Thermal Engineering*

Received Date: 6 April 2009
Accepted Date: 28 November 2009

Please cite this article as: B. Končar, P. Norajitra, K. Oblak, Effect of nozzle sizes on jet impingement heat transfer in He-cooled divertor, *Applied Thermal Engineering* (2009), doi: 10.1016/j.applthermaleng.2009.11.018

Effect of nozzle sizes on jet impingement heat transfer in He-cooled divertor

Boštjan Končar*[1], Prachai Norajitra[3], Klemen Oblak[2]

[1]Jožef Stefan Institute, Reactor Engineering Division

Jamova 39, SI- 1000 Ljubljana

*bostjan.koncar@ijs.si

[2]University of Ljubljana, Faculty of Mechanical Engineering

Aškerčeva 6, SI-1000 Ljubljana

[3]Forschungszentrum Karlsruhe, Institute for Material Research III

P.O. Box 3640, D 76021 Karlsruhe

*Corresponding Author:

Boštjan Končar

Adress: Jožef Stefan Institute, Reactor Engineering Division, Jamova 39, SI- 1000 Ljubljana

Tel: +386 1 5885 260

Fax: +386 1 5885 377

E-mail: bostjan.koncar@ijs.si

ABSTRACT

The use of impinging jets for divertor cooling in the conceptual fusion power plant is attracting much attention due to its very high heat removal capability and moderate pumping power requirement. The latest and the most advanced divertor concept is based on modular design cooled by helium impinging jets. To reduce the thermal stresses, the plasma-facing side of the divertor is build up of numerous small cooling fingers cooled by an array of helium jets. In this study the influence of nozzle sizes on the heat transfer and flow characteristics of such cooling finger is investigated numerically. The main objective is to find an optimal size and distribution of nozzle diameters in the jet array in which the heat transfer would be the highest possible at an acceptable pressure drop through the cooling finger. Prior to nozzle diameters modification, the simulation results for the reference finger geometry were validated against high heat flux experiments. A good agreement was obtained. The nozzle diameters were then modified at two different mass flow rates (13.5 g/s and 6.8 g/s per cooling finger). The most critical design parameter of interest was the maximum thimble temperature, which is limited by the melting temperature of the filler material in the brazed finger joint. It has been found that an optimal jet arrangement should have equal nozzle diameters to reach the highest thimble temperature decrease, while keeping the pressure drop within reasonable limits.

KEYWORDS

helium-cooled divertor, jet impingement, nozzle diameter, numerical analyses

1 Introduction

The divertor is one of the high-heat-flux components in a fusion reactor. Its main function is to remove the fusion reaction ash, unburned fuel, and eroded particles from the reactor first wall, which adversely affect the quality of the plasma. About 15 % of the total thermal power gained from the fusion reaction need to be removed by divertor, which results in an extremely high heat flux applied on a relatively small divertor target plate. Different helium-cooled divertor concepts, described in [1], have been proposed for a fusion power plant application. A modular helium-cooled divertor for post-ITER generation of fusion reactors has been developed at Forschungszentrum Karlsruhe (FZK) [2, 3]. Its main design requirement is to remove high heat flux loads of 10 to 15 MW/m^2. Usage of helium as a coolant simplifies the balance of the power plant as the same coolant can be used for all internal components. Helium loop has also favorable safety characteristics, but is capable of efficient heat transfer only if operated at high pressure (10 MPa in the current design). It's comparatively low heat removal capability can be improved by heat transfer enhancement methods, such as jet impingement [4]. Jet impingement heat transfer is a well-known heat transfer enhancement technique that has found an extensive use in industrial application for aircraft engines, burners, gas turbine blades, cooling of electronic components, etc. When jets are used in arrays they are ideal for global cooling of the heated surface [5].

Impingent by multiple jets can be easily adapted also for cooling of the divertor target plate. The latest design of the helium cooled divertor uses small tungsten cooling fingers, cooled by high pressure helium impinging jets (Figure 1) [6]. The design concept with multiple helium jets is denoted as HEMJ (Helium-cooled Multiple-Jet) design. To optimize the HEMJ design, the analyses with Computational Fluid Dynamics (CFD) programs are

necessary [7]. By the help of the numerical analyses the local critical regions in the design can be identified and thus help to reduce the number of expensive experiments.

In this work the size and distribution of nozzles on the cartridge was optimized for the reference geometry of one cooling finger. The effect of nozzle diameters on the heat transfer and pressure drop characteristics was investigated. Diameters of the nozzles were varied at two different mass flow rates, 13.5 g/s and 6.8 g/s (characteristic for fusion reactor operating conditions). The heat removal ability and pressure drop is analyzed in detail for lower mass flow rate.

2 Divertor cooling finger – reference design and numerical model

The reference finger design denoted as J1-C [6] was used as a basis for parametric analyses of nozzle diameters variation. The plasma-facing side of the divertor (target plate) is constructed of small hexagonal tungsten tiles. Each tile is brazed on the thimble, made of tungsten alloy W-1%La_2O_3 (WL10). A steel cartridge with 25 nozzles on the top of it is inserted in the thimble. The helium jets under high pressure blow through these nozzles and cool the hot inner surface of the thimble. The geometry of the reference design is shown in Figure 1. The tile width is 17.8 mm, the thimble thickness is 1.03 mm and the outer diameter of the cartridge is 11.2 mm. The nozzles on the top of the cartridge have the diameter of 0.6 mm, except for the central nozzle with the diameter of 1.04 mm. The gap between the thimble and cartridge is 0.9 mm.

PLACE FIGURE 1 HERE.

This geometry was found as a result of previous studies [6], where base geometrical parameters (geometry of the tile and the thimble, the gap size, the number and arrangement of nozzles on the cartridge) were determined to accommodate for a heat flux of at least 10

MW/m^2. The heat transfer and flow characteristics of the reference design were also experimentally tested and numerically validated in an air flow loop under a wide range of Reynolds numbers but at much lower heat fluxes (up to 1 MW/m^2) [8]. The main goal of optimization studies is to cool down the divertor structures as much as possible and at the same time limit the pressure drop to reasonable values to save pumping power. One of the most critical design limits is the maximum allowable temperature of the thimble dictated by the re-cristallization temperature of the WL10 material (currently assumed at 1300°C under irradiated condition). In this respect the geometry should be further optimized to enhance the heat transfer and, hence, to enlarge the safety margin. In this work, the design modification is focused on optimization of the size and distribution of nozzle diameters on the cartridge.

Heat transfer performance of different cartridge design variants are analyzed numerically using the code ANSYS-CFX 11.0 [9]. Taking into account the symmetry of the cooling finger, a 30^o periodic segment of the finger is being simulated. Numerical domain consists of 3 solid domains (tile, thimble, cartridge) and of one fluid domain. Heat transfer equations through solid and fluid are solved simultaneously. The transport processes are assumed to be at steady-state. In the fluid domain, the helium is modeled as an ideal gas. The following transport equations are solved in the fluid domain:

continuity equation

$$\nabla \cdot (\rho \vec{v}) = 0\,, \quad (1)$$

momentum equation

$$(\vec{v} \cdot \nabla)\vec{v} = -\nabla p + \vec{g} + (\mu + \mu_t)\nabla^2 \vec{v}\,, \quad (2)$$

and energy equation

$$\rho(\vec{v}\cdot\nabla U)-\nabla\cdot(\lambda\nabla T)+p\nabla\cdot\vec{v}=0\,, \quad (3)$$

where ρ, $\vec{v}$, U, p, μ, μ_t, $\vec{g}$, λ, T are helium density, velocity, internal energy, pressure, dynamic viscosity, turbulent viscosity, gravity force density, thermal heat conductivity of the helium and temperature, respectively. Shear stress transport (SST) two-equation turbulence model [10] has been used to resolve turbulence and heat transfer scales in the helium flow. The SST formulation combines k-ω model to resolve near-wall turbulence and k-ε model for the bulk flow. In the solid domain the heat conduction equation for steady-state conditions is solved:

$$\nabla\cdot(\lambda_s\nabla T_s)=0\,, \quad (4)$$

where ρ_s, c_s, T_s and λ_s are the density, specific heat capacity and thermal conductivity of the solid, respectively. The material properties of the tile and the thimble are modeled as temperature-dependent according to the ITER Material Properties Handbook [11]. Due to low temperature gradients in the steel cartridge, its material properties are taken at constant temperature. Constant heat flux is applied at the upper surface of the tile and adiabatic boundary conditions are assumed at the outer walls. Helium flow enters the cartridge at the constant mass flow rate.

The flow field and the structures are meshed by hexagonal mesh with about 400,000 cells, as shown in Figure 2. The mesh refinement is applied especially in near-wall region at the helium-thimble interface, where the highest velocity and temperature gradients occur. Our previous analyses [12] have shown that this mesh is sufficient to obtain mesh independent results. Hexagonal mesh was constructed in ANSYS Multiphysics program package [13] in a parametrical way that enables automatic mesh generation based on

predefined geometry dimensions and mesh refinement parameters. Such parametrization enabled fast mesh generation for different design changes used in this study.

PLACE FIGURE 2 HERE.

3 Validation against experimental data

To have confidence in CFD results, the numerical simulations were first verified against the experimental data. The high heat flux experiments with the reference cooling finger mock-up were performed at the experimental facility located at the Efremov Institute, St. Petersburg, Russia [14]. The facility consists of the electron beam (60 kW at 27 keV beam energy) and of the helium loop (see Figure 3). Powerful electron beam gun enables testing of mock-ups at high heat fluxes up to 15 MW/m^2.

The data for validation of numerical results were extracted from the first test series, performed in 2006 [15]. During the tests thermo-cyclic loading was applied to the tile upper surface aiming to test the integrity of divertor materials. Thermo-cycles were simulated by switching the beam on and off. For the selected test case the thermo-cyclic loading was applied at five heat flux levels. At each heat flux level, 10 cycles were performed. The helium mass flow rate was kept approximately constant at about 13.5 g/s.

To validate steady-state CFD simulations, the data were extracted at different heat flux levels, during the time intervals, when the laser beam was switched on. The measured parameters are presented in Table 1. Tile surface temperatures were measured by infrared (IR) camera.

PLACE FIGURE 3 HERE.

PLACE TABLE 1 HERE.

A 30^{o} segment of one-finger module with hexagonal mesh (see Figure 2) was used to simulate experiments from Table 1. It should be noted that the tile size of experimental mock-up is slightly different than the tile size of reference design from Figure 1. Namely, the tile width of the experimental mock-up is 17.2 mm (as compared to 17.8 mm for the reference design).

Simulation results and measured data are compared in Figure 4. The critical quantity of interest is the maximum thimble temperature. Two critical values should be considered. The first one is the re-cristallization temperature of the thimble material WL10 (1300 ^{o}C) and the other limitation is the melting temperature of the brazing filler material. Tile and thimble are brazed together with STEMET 1311®, which has a melting temperature at about 1050 ^{o}C. The helium mass flow rate was rather high (~13.5 g/s) to keep the temperature at the tile/thimble brazed joint below 1050 ^{o}C. As shown in Figure 4 (right), a reasonable agreement between the measured and calculated tile surface temperature has been obtained. The experimental heat flux in Table 1 was re-calculated from the measured helium temperature difference (the removed heat is absorbed in helium) to exclude the errors due to beam reflection and due to heat losses through the flange, where the mock-up is fixed (the real boundary condition in the experiment is not completely adiabatic). The calculated thimble temperature exceeds the allowable temperature of 1050 ^{o}C for the highest heat flux value 12.62 MW/m^2. The post-test metallographic examination of the mock-up confirmed tile detachment, which indicates that the tile-thimble brazing temperature was exceeded also in the experiment [15].

PLACE FIGURE 4 HERE.

4 Effect of nozzle diameters

4.1 Parametric analysis of nozzle diameters at high mass flow rate of 13.5 g/s

The main objective is to reduce the maximum thimble temperature by changing the nozzle diameters on the cartridge. At the same time the increase of the pressure drop should be as low as possible. Various experimental and numerical investigations have shown that optimized nozzle geometric parameters may improve the heat transfer and flow characteristics of impinging jets [4,5,16,17]. The reference geometry of the cooling finger (see Figure 1) was used as a basis to perform parametric analysis of cartridge design changes. Diameters of the nozzles were varied, whereas other geometry parameters remained unchanged. The hexagonal mesh as shown in Figure 2 was used for all cartridge designs. Modified cartridge geometries require minor mesh adaptation perpendicular to the jet flow. Mesh accommodation itself has no significant effect on the results. Parametric calculations were performed for the reference scenario without internal heating (similar to Efremov experiments). The following boundary conditions were adopted:

- He mass flow rate: 13.5 g/s
- He inlet temperature: 540 °C
- He inlet pressure: 10.0 MPa
- Heat flux: 11.6 MW/m^2

In the first set of modifications, the diameter of the central nozzle was varied from 0.6 mm up to 1.3 mm whereas in the second set (case1 to case4) also the other nozzles were modified (see Table 2). For cases 1 to 4, the total jets cross section area was kept constant, which resulted in a very small change of the pressure drop. For all cases the minimum

nozzle diameter was limited to 0.6 mm to avoid potential danger of a blockage. Nozzles are arranged in four circular rows around the central nozzle as shown in Figure 5.

PLACE FIGURE 5 HERE.

In Table 2, the comparison of pressure drop and maximum tile and thimble temperatures are presented. The values of maximum thimble temperature change and pressure drop change are calculated with regard to the reference cartridge design (gray column). The lowest thimble temperature decrease of approximately 20 ^{o}C was achieved at the smallest central nozzle diameter, but in that case the pressure drop increased by 82 kPa.

PLACE TABLE 2 HERE.

For constant jets cross-section, the change in the pressure drop is much lower (3.8 to 12.8 kPa) than for the first set of design changes (-42.8 to 82 kPa). In Figure 6 the maximum thimble and tile temperatures for different design modifications are plotted with respect to the calculated pressure drop. As shown, the decrease in material temperature is closely associated with the increased pressure drop. Different trend of design modifications is presented by red (constant jets cross section) and blue (change of central nozzle diameter) lines. Steeper slope of the red line shows that the thimble temperature decrease per pressure drop is higher for the nozzle variations at the constant jets cross section area.

PLACE FIGURE 6 HERE.

4.2 Parametric analysis of nozzle diameters at nominal mass flow rate of fusion reactor

Sensitivity analysis of different nozzle diameters has been performed also for lower mass flow rate conditions, characteristic for fusion power plant operating conditions. Here, the mass flow rate per one cooling finger was reduced to 6.8 g/s. The parametric analysis of

nozzle diameters is performed in the same way as for the higher mass flow rate. The results are presented in Table 3 and in Figures 7 to 11. As shown in Table 3 the maximum tile and thimble temperatures are expectedly higher for lower mass flow rate resulting in 5 times lower pressure drop (about 113 kPa) for the reference design. The pressure drop change at the central nozzle variation ranges from -10.8 kPa to 17.6 kPa, whereas it is practically negligible for nozzle variations at the constant jets cross section area.

PLACE TABLE 3 HERE.

The maximum thimble temperature versus the pressure drop for different designs is shown in Figure 7. Different trend of design modifications is presented by red (constant jets cross section) and blue (central nozzle diameter change) lines. The slope of the red line is steeper and thus indicates that the design modifications at constant jets cross section cause much higher thimble temperature change at the same pressure drop change. On the other hand, this also means that the thimble temperature is very sensitive to a small change in diameter (in the range of manufacturing accuracy). The comparison of Figures 5 and 6 further shows that the thimble temperature decrease per pressure drop is much higher at a lower mass flow rate.

PLACE FIGURE 7 HERE.

The temperature distribution in the solid parts (tile, thimble, cartridge) and in the helium flow channel is presented on Figure 8 (left). The maximum tile temperature occurs on the heated surface, at the tile outer corner. The maximum thimble temperature is just above the central jet, on the tile-thimble interface. The right side of Figure 8 shows the distribution of the local heat transfer coefficient at the fluid-thimble interface. As shown, the local heat transfer peaks occur in the jet regions. The local heat transfer coefficient is defined as:

$$HTC = \frac{q_{w,i}}{(T_{w,i} - T_{f,inlet})}, \quad (5)$$

where $q_{w,i}$, $T_{w,i}$ and $T_{f,inlet}$ are the local wall heat flux, the local wall temperature at the fluid-thimble interface and inlet temperature of the fluid, respectively.

PLACE FIGURE 8 HERE.

The influence of design changes on the local heat transfer distribution is presented in Figure 9. To compare heat transfer coefficients, the distribution of local HTC values along the two polylines is plotted for each design. Polylines are defined at the thimble-fluid interface on the front and the back side of the 30^o segment (see Figure 7). As shown in Figure 9, each local HTC peak approximately corresponds to the local jet region. The lowest peak occurs near the central jet region and is shifted from the centre for about 0.5 mm.

Smaller diameter of the central nozzle tends to increase the heat transfer coefficient peak in the central jet region. Smaller central nozzle also increases the second HTC peak in the first row and shifts it towards the centre. The design changes at the constant jets cross section show similar tendency versus the reference design. The first HTC peak is still somewhat lower than the second one. Considering only the HTC distribution, the best results have been obtained for the design with the smallest central nozzle of 0.6 mm.

PLACE FIGURE 9 HERE.

HTC distribution at the fluid-thimble interface strongly depends on the local flow conditions in each of the nozzle. Figure 10 shows Reynolds numbers and average nozzle velocities for each of the nozzle rows on the cartridge. Three different designs (1.04 (reference), 0.6 and case3) from Table 3 are compared. Nozzle velocities are averaged over the cross-section of the nozzle exit. As shown in Figure 10 (left), the highest Re number

(22700) occurs in the central nozzle of the reference design (1.04). This is mainly due to the larger diameter of the central nozzle (1.04 mm). Reynolds numbers for the other two designs with equal nozzle diameters are much more evenly distributed over the nozzles and are around 15000. When only designs 0.6 and case3 are compared, the Re numbers for the design 0.6 are slightly higher for all nozzle rows. The main reason lies in higher nozzle velocities for the design 0.6, which has smaller nozzle cross-sections than the case3 at the same mass flow rate. This is clearly shown in Figure 10 (right) representing the nozzle velocities. The jet through the central nozzle is the most important for reduction of the maximum temperature in the thimble material. Higher central jet velocity contributes to the increased heat removal ability in the central region. As shown in Figure 10 (right), the highest velocity through the central nozzle (160 m/s) is obtained for the design 0.6. On the other hand the lowest velocity is obtained for the reference design 1.04. The designs 1.04 and case3 have equal cross-sections therefore here the effect of design change on the nozzle velocity re-distribution may be analyzed. Figure 10 (right) shows that the decreased central nozzle diameter (case 3 design) reduces the velocities in the first row on account of increased velocity through the central nozzle. The highest nozzle velocities are obtained in the forth row on the edge of the cartridge.

PLACE FIGURE 10 HERE.

Since the highest local temperatures at the fluid-thimble interface appear in the central jet region, the local HTC value in the centre was selected as the most representative to evaluate the heat removal ability of the HEMJ design. The local HTC values are listed in Table 3 and presented in Figure 11 (left) versus the pressure drop. HTC in the centre increases almost linearly with decreasing of central nozzle diameter and pressure drop. On the other hand the pressure drop remains almost the same for designs with constant jets

cross section, but the heat transfer coefficient still increases. Case1 and Case3 designs show the highest HTC values in that respect.

To evaluate and classify the heat removal ability versus the helium flow resistance for different designs, the "divertor efficiency" is given as the ratio between the HTC in the centre and the overall pressure drop. The divertor efficiency versus the central nozzle diameter is shown in Figure 11 (right). The highest efficiency was achieved for Case3 design (equal nozzle diameters at constant jets cross section). At central nozzle diameter changes, the best result is achieved for 0.6 mm nozzle (also in this case all nozzle diameters are the same). This is also the most attractive solution from the point of view of reaching the highest thimble temperature reduction of around 30^{o}C, while keeping the pressure drop within reasonable limits. The decrease of thimble temperature for this case is more than 27 ^{o}C and the pressure drop is still acceptable at 130 kPa. (see Table 3).

PLACE FIGURE 10 HERE.

5 Conclusions

CFD analyses were used to optimize the nozzle diameters on the cartridge of the reference divertor cooling finger. To gain confidence in simulation results, they were first verified against the high heat flux experiments. The calculated and measured values of the tile surface temperature show good agreement. The cartridge design optimization was focused on variation of nozzle diameters at two different mass flow rates, 13.5 g/s and 6.8 g/s (the lower value is characteristic for fusion power plant operating conditions). The most critical design parameter of interest was the maximum thimble temperature. The heat transfer characteristics and pressure drop have been analyzed in detail at a lower mass flow rate. The main findings of this analysis can be summarized as follows:

- By increasing the diameter of the central nozzle, the maximum thimble temperature increases linearly, whereas the pressure loss trend shows linear decrease.
- In the second series of design changes, all nozzle diameters were varied, while keeping the jets cross section area constant. For this type of design changes, the pressure drop change was considerably lower or even negligible for a lower mass flow rate.
- Maximum thimble temperature decrease per pressure drop is much higher at the lower mass flow rate. At the lower mass flow rate conditions, the thimble temperature is very sensitive even to a very small change of nozzle diameter (in the range of manufacturing accuracy). The effect of the design change on the pressure drop is more important at higher mass flow rates.
- Analysis of local flow conditions in the jet array shows that the smaller central nozzle diameter contributes to higher central jet velocity and consequently to reduction of the maximum temperature of the thimble material.
- Local heat transfer coefficient in the centre and overall pressure drop through the finger appear to be the most appropriate parameters to characterize the design from the heat removal and thermohydraulic point of view. To evaluate the performance of different design changes, the "divertor efficiency" was introduced as the ratio between heat transfer coefficient in the centre and overall pressure drop.
- The highest divertor efficiency was achieved for the design with equal nozzle diameters at constant jets cross section (Case3).
- The reference design (central nozzle diameter of 1.04 mm) showed the lowest efficiency amongst all proposed design changes.

- The highest thimble temperature reduction of around 27 ^{o}C was achieved for the cartridge design with equal nozzle diameters of 0.6 mm.

ACKNOWLWDGEMENTS

This work, supported by the European Commission and the Slovenian Research Agency was carried out within the framework of European Fusion Development Agreement (EFDA).

REFERENCES

[1] A.R. Raffray, S. Malang, X. Wang, Optimizing the overall configuration of a He-cooled W-alloy divertor for a power plant, Fusion Engineering and Design 84 (2009) 1553-1557.

[2] R. Kruessman, P. Norajitra (Eds.), Conceptual design of a He-cooled divertor with integrated flow and heat transfer promoters (PPCS subtask TW3-TRP-001-D2), Part II: Detailed Version. Forschungszentrum Karlsruhe, Scientific Report, FZKA 6975, April 2004.

[3] P. Norajitra et al., He-cooled Divertor for DEMO: Experimental Verification of the Conceptual Modular Design, Fusion Engineering Design 81 (2006), 341-346.

[4] E. Baydar, Y. Ozmen, An experimental and numerical investigation on a confined impinging air jet at high Reynolds numbers, Applied Thermal Engineering, 25 (2008) 409-421.

[5] B.P. Whelan, A.J. Robinson, Nozzle geometry effects in liquid jet array impingement, Applied Thermal Engineering, Article in press (2008).

[6] P. Norajitra, et al., He-cooled divertor development for DEMO, Fusion Engineering Design 82 (2007) 2740–2744.

[7] T. Ihli, et al., An advanced He-cooled divertor concept: Design, cooling technology, and thermohydraulic analyses with CFD, Fusion Engineering and Design 75-79 (2005) 371-375.

[8] J.B.Weathers, et al., Development of modular helium-cooled divertor for DEMO based on the multi-jet impingement (HEMJ) concept: Experimental validation of thermal performance, Fusion Engineering Design 83 (2008) 1120–1125.

[9] ANSYS CFX, Release11.0, ANSYS CFX-Solver Theory Guide, ANSYS, 2006.

[10] F.R Menter., Multiscale model for turbulent flows, 24th Fluid Dynamics Conference, 1986, American institute of aeronautics and astronautics.

[11] ITER Material Properties Handbook, 2001.

[12] B. Končar, et al., Numerical Investigation of Multiple-Jet Cooling Concept for Helium Cooled Divertor, International Conference Nuclear Energy for New Europe 2008, Portorož, Slovenia.

[13] P. Kohonke, et al., Ansys Inc., Theory Reference, Ansys Inc., Southpointe 275 Technology Drive Canonsburg, PA 15317, 2004.

[14] I. Ovchinnikov, et al., Experimental study of DEMO helium cooled divertor target mock-ups to estimate their thermal and pumping efficiencies, Fusion Engineering and Design 73 (2005) 181–186.

[15] R. Giniytulin, et al., Manufacturing and testing the He-cooled target module mock-ups for DEMO fusion reactor divertor, Status report, EFREMOV Institute STC Sintez St. Peterburg, 2006.

[16] Z.Q. Luo, A.S. Mujumdar, C. Yap, Effects of geometric parameters on confined impinging jet heat transfer, Applied Thermal Engineering, 25 (2008) 2687-2697.

[17] L.A. Brignoni, S.V. Garimella, Effects of nozzle-inlet chamfering on pressure drop and heat transfer in confined air jet impingement, Int. J. Heat Mass Transfer 31 (2004) 251-260.

TABLES

Table 1 Measured parameters during thermo-mechanical tests of HEMJ#J1-C [16]

$q_{(dT\ He)}$ [MW/m^2]	$\dot{m}_{He}$ [g/s]	$p_{(He\ inlet)}$ [MPa]	Δp [kPa]	$T_{(He\ inlet)}$ [^{o}C]	ΔT_{He} [^{o}C]	$T_{Tile\text{-}surf.\ max}$ [^{o}C]
4.01	13.06	9.61	326.7	523.6	15.3	941
6.28	13.7	9.79	321.2	536.9	22.8	1153
9.69	13.73	9.69	326.6	555.4	35.1	1424
11.63	13.7	9.84	327.4	558.9	42.2	1597
12.62	13.28	9.72	313.3	567.8	47.2	1788

Table 2 Variation of nozzle diameters at mass flow rate 13.5 g/s

	Reference	0.6	0.8	1.3	Case 1	Case 2	Case 3	Case 4
$D_{centr.\ jet}$ [mm]	1.04	0.6	0.8	1.3	0.6	0.75	0.6236	0.7
$D_{1.\ row}$ [mm]	0.6	0.6	0.6	0.6	0.69	0.65	0.6236	0.65
$D_{2.\ row}$ [mm]	0.6	0.6	0.6	0.6	0.6035	0.62	0.6236	0.63
$D_{3.\ row}$ [mm]	0.6	0.6	0.6	0.6	0.6	0.6	0.6236	0.6
$D_{4.\ row}$ [mm]	0.6	0.6	0.6	0.6	0.6	0.6	0.6236	0.6
$T_{max,\ Tile}$ [oC]	1,670.85	1,656.5	1,661.6	1,679.6	1,667.8	1,670.2	1,668.6	1,670.3
$T_{max,\ Thim.}$ [oC]	1,016.85	997.5	1,004.1	1,029.2	1,008.8	1,012.2	1,010.7	1,011.9
$T_{He,out}$ [oC]	584.85	584.7	584.2	584.7	584.2	584.4	584.3	584.0
Δp [kPa]	430.00	512.0	472.9	387.2	442.8	435.0	437.3	433.8
$d\Delta p$ [kPa]	/	82.0	42.9	-42.8	12.8	5.0	7.3	3.8
$dT_{max,Thim.}$ [oC]	/	-19.4	-12.7	12.4	-8.0	-4.6	-6.1	-4.9
A_{jets} [mm^2]	7.64	7.07	7.29	8.11	7.64	7.64	7.64	7.64

Table 3 Variation of nozzle diameters at mass flow rate 6.8 g/s

	Reference	0.6	0.8	1.3	Case 1	Case 2	Case 3	Case 4
$D_{centr.\ jet}$ [mm]	1.04	0.6	0.8	1.3	0.6	0.75	0.6236	0.7
$D_{1.\ row}$ [mm]	0.6	0.6	0.6	0.6	0.69	0.65	0.6236	0.65
$D_{2.\ row}$ [mm]	0.6	0.6	0.6	0.6	0.6035	0.62	0.6236	0.63
$D_{3.\ row}$ [mm]	0.6	0.6	0.6	0.6	0.6	0.6	0.6236	0.6
$D_{4.\ row}$ [mm]	0.6	0.6	0.6	0.6	0.6	0.6	0.6236	0.6
$T_{max,\ Tile}$ [oC]	1,874.2	1,849.9	1,859.1	1,890.6	1,873.6	1,873.3	1,869.9	1,868.9
$T_{max,\ Thim.}$ [oC]	1,202.3	1,175.1	1,185.3	1,223.2	1,199.0	1,198.0	1,196.2	1,193.7
$T_{He,out}$ [oC]	625.2	624.3	624.9	626.4	624.6	625.0	624.0	625.0
Δp [kPa]	112.8	130.4	122.5	100.7	113.2	113.1	113.0	114.5
$d\Delta p$ [kPa]	/	17.6	9.6	-12.1	0.4	0.3	0.2	1.6
$dT_{max,Thim.}$ [oC]	/	-27.2	-17.0	21.0	-3.2	-4.2	-6.0	-8.6
HTC_{center} [W/m^2K]	28,490	35,236	31,521	25,821	34,209	31,753	33,950	32,338
$HTC/\Delta p$ [W/m^2KkPa]	252.55	270.20	257.40	256.49	298.91	280.43	300.36	285.85

FIGURE CAPTIONS

Figure 1 Divertor cooling finger

Figure 2 Numerical mesh of the 30^{o} segment of the cooling finger

Figure 3 Testing facility at Efremov Institute [14]

Figure 4 He temperature difference and pressure drop in the helium loop (left); maximum tile and thimble temperatures (right)

Figure 5 Distribution of nozzles in the cartridge

Figure 6 Maximum thimble and tile temperatures vs. pressure drop due to changed diameter of the nozzles

Figure 7 Maximum thimble temperature vs. pressure drop due to changed nozzle diameters (at 6.8 g/s)

Figure 8 Temperature distribution (left) and wall heat transfer at the fluid-thimble interface (right) at DEMO mass flow rate of 6.8 kg/s

Figure 9 HTC values at fluid-thimble interface at mass flow rate 6.8 g/s

Figure 10 Nozzle Reynolds numbers (left) and average nozzle velocities (right) affected by different designs at mass flow rate 6.8 g/s

Figure 11 HTC above the central jet (left) and thermalhydraulic performance (right) of design changes at mass flow rate 6.8 g/s – variation of central nozzle diameter (blue ticks) vs. variation of all nozzle diameters at constant jets cross section (red ticks)

FIGURES

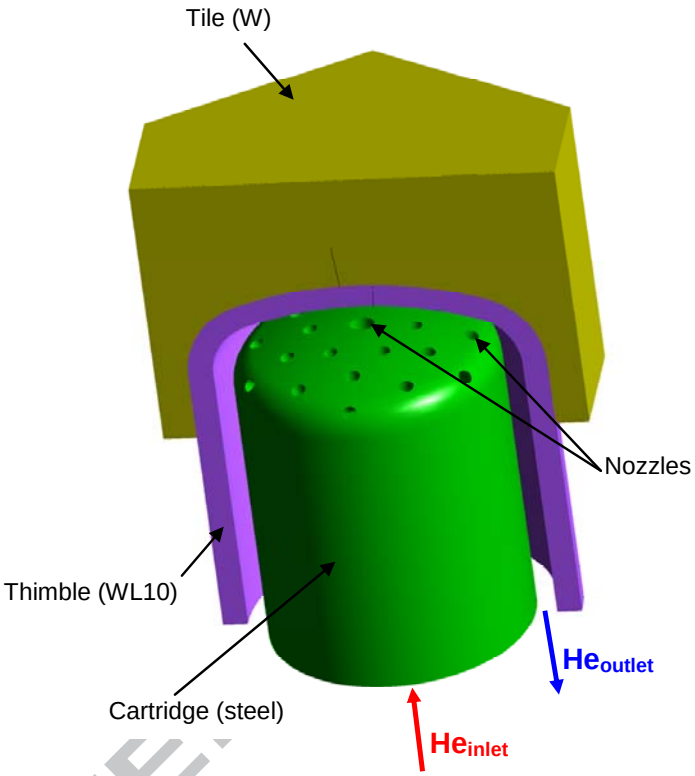

Figure 1 Divertor cooling finger

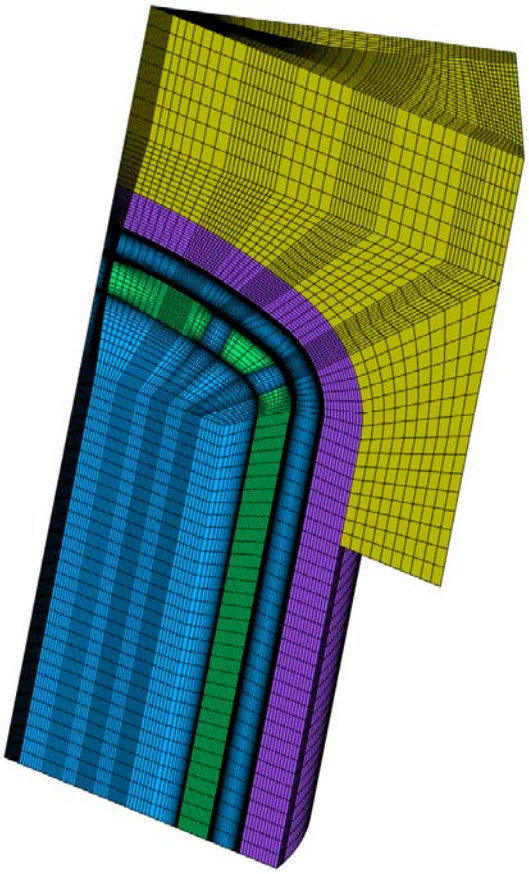

Figure 2 Numerical mesh of the 30^{o} segment of the cooling finger

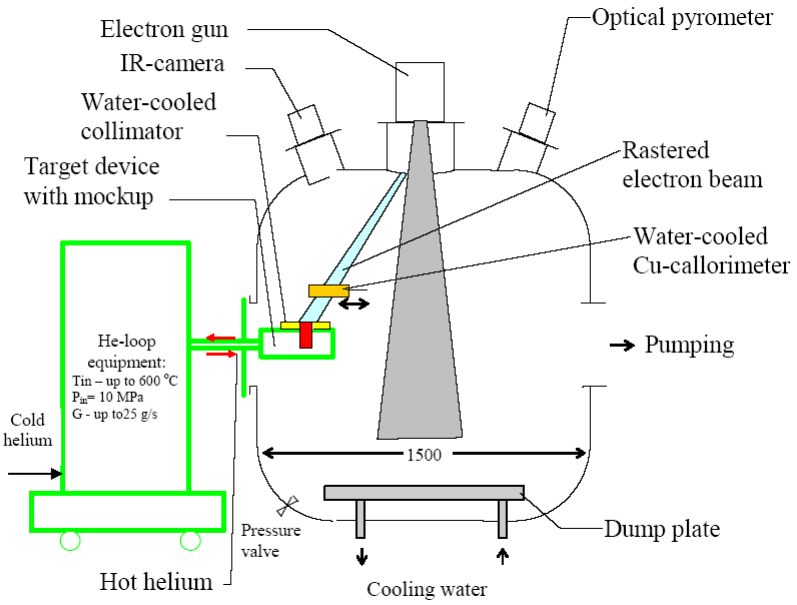

Figure 3 Testing facility at Efremov Institute [14]

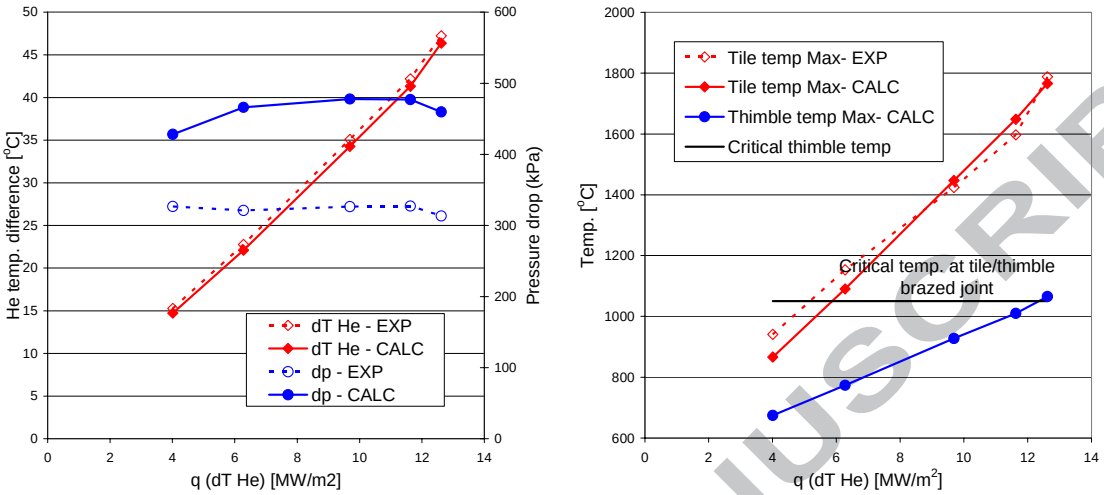

Figure 4 He temperature difference and pressure drop in the helium loop (left); maximum tile and thimble temperatures (right)

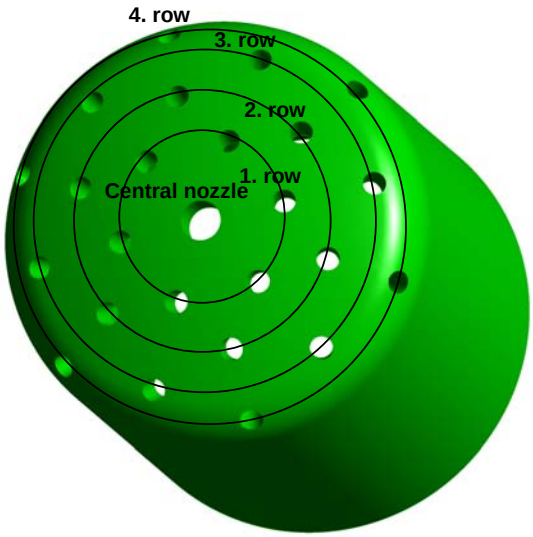

Figure 5 Distribution of nozzles in the cartridge

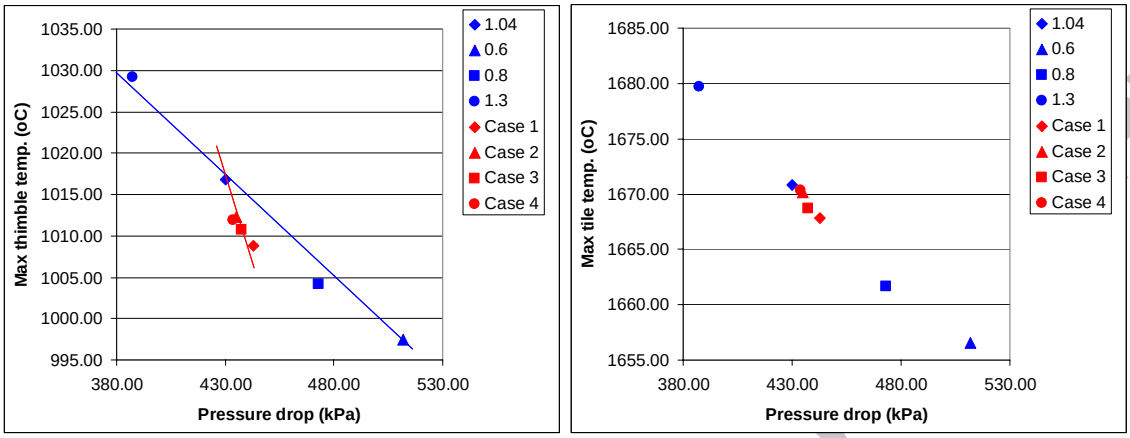

Figure 6 Maximum thimble and tile temperatures vs. pressure drop due to changed diameter of the nozzles

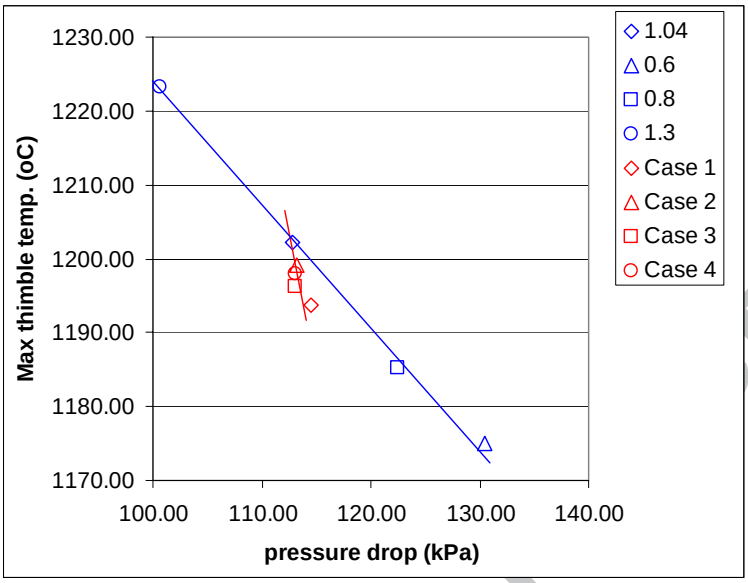

Figure 7 Maximum thimble temperature vs. pressure drop due to changed nozzle diameters (at 6.8 g/s)

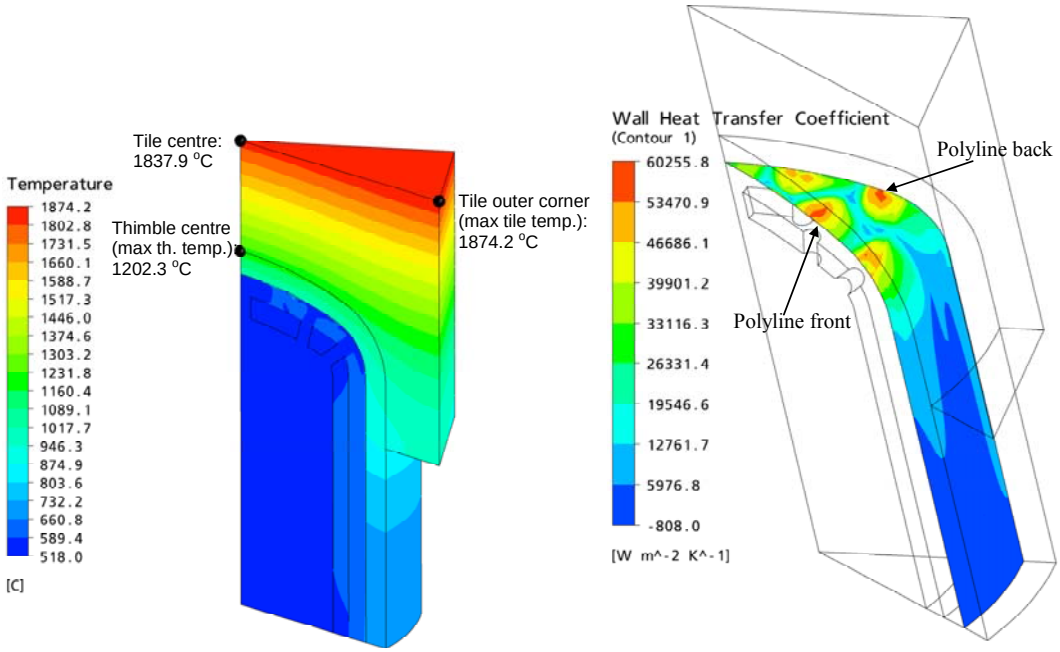

Figure 8 Temperature distribution (left) and wall heat transfer at the fluid-thimble interface (right) at DEMO mass flow rate of 6.8 kg/s

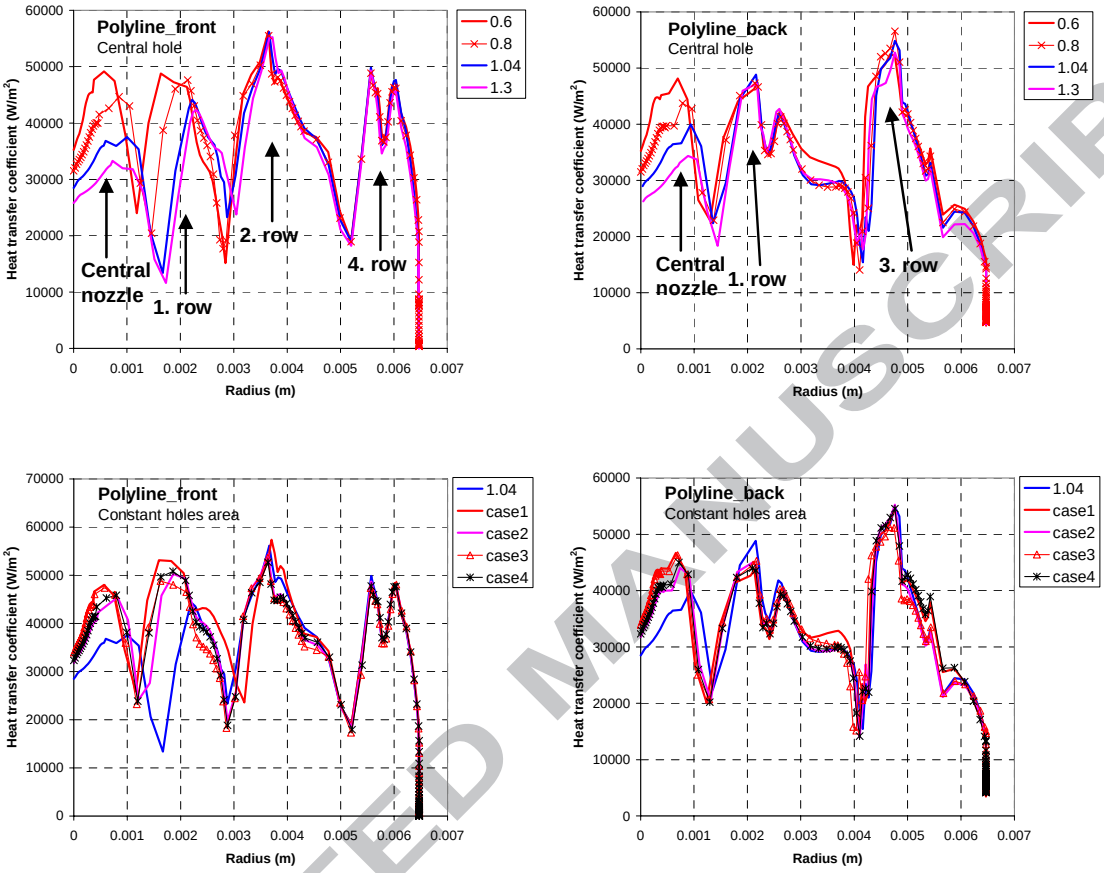

Figure 9 HTC values at fluid-thimble interface at mass flow rate 6.8 g/s

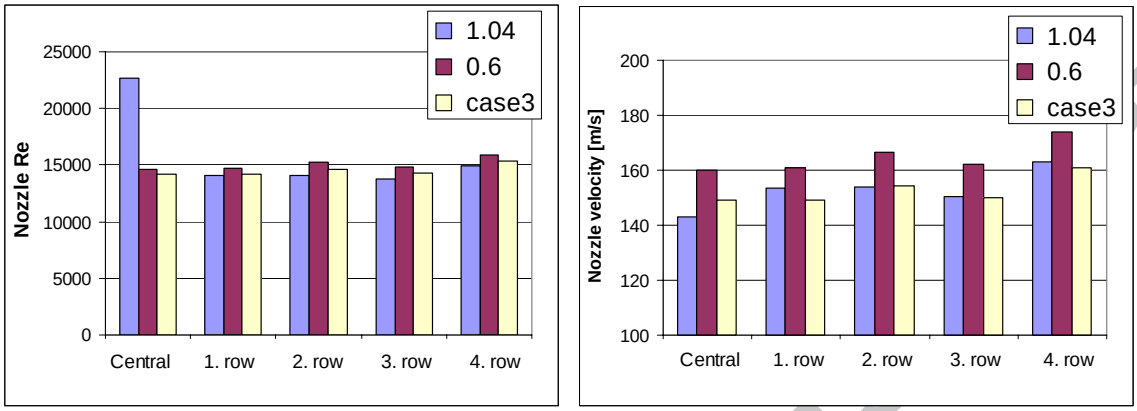

Figure 10 Nozzle Reynolds numbers (left) and average nozzle velocities (right) affected by different designs at mass flow rate 6.8 g/s

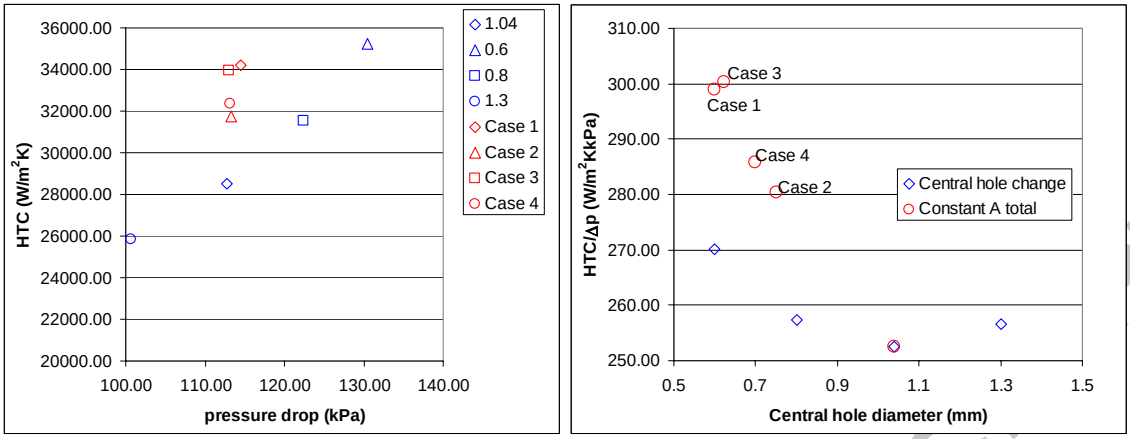

Figure 11 HTC above the central jet (left) and thermalhydraulic performance (right) of design changes at mass flow rate 6.8 g/s – variation of central nozzle diameter (blue ticks) vs. variation of all nozzle diameters at constant jets cross section (red ticks)